Progress in Oceanography 162 (2018) 290–302

Contents lists available at ScienceDirect

Progress in Oceanography

journal homepage: www.elsevier.com/locate/pocean

Modeling investigation of the nutrient and phytoplankton variability in the Chesapeake Bay outflow plume

Long Jiang, Meng Xia*

Department of Natural Sciences, University of Maryland Eastern Shore, Princess Anne, MD 21853, USA

ARTICLE INFO

Keywords:
Chesapeake Bay outflow plume (CBOP)
Nutrient limitation
Phytoplankton
River discharge
Winds

ABSTRACT

The Chesapeake Bay outflow plume (CBOP) is the mixing zone between Chesapeake Bay and less eutrophic continental shelf waters. Variations in phytoplankton distribution in the CBOP are critical to the fish nursery habitat quality and ecosystem health; thus, an existing hydrodynamic-biogeochemical model for the bay and the adjacent coastal ocean was applied to understand the nutrient and phytoplankton variability in the plume and the dominant environmental drivers. The simulated nutrient and chlorophyll *a* distribution agreed well with field data and real-time satellite imagery. Based on the model calculation, the net dissolved inorganic nitrogen (DIN) and phosphorus (DIP) flux at the bay mouth was seaward and landward during 2003–2012, respectively. The CBOP was mostly nitrogen-limited because of the relatively low estuarine DIN export. The highest simulated phytoplankton biomass generally occurred in spring in the near field of the plume. Streamflow variations could regulate the estuarine residence time, and thus modulate nutrient export and phytoplankton biomass in the plume area; in comparison, changing nutrient loading with fixed streamflow had a less extensive impact, especially in the offshore and far-field regions. Correlation analyses and numerical experiments revealed that southerly winds on the shelf were effective in promoting the offshore plume expansion and phytoplankton accumulation. Climate change including precipitation and wind pattern shifts is likely to complicate the driving mechanisms of phytoplankton variability in the plume region.

1. Introduction

Plumes are the mixing interface between the riverine/estuarine and shelf waters (Dagg et al., 2004; Herrmann et al., 2015). Riverine waters carry a considerable amount of inorganic and organic nutrients, and are generally more turbid and biologically productive than shelf waters; thus, the plume region is usually associated with extensive nutrient transformation, active biological activities, and complex biophysical controls (Boicourt et al., 1987). Moreover, the plume frontal zone provides excellent nursery habitats for larval fish due to its special water motions (convergence and retention), superior feeding conditions, and relatively low predation pressure (Grimes and Kingsford, 1996). Sitting at the base of the food web, phytoplankton play a fundamental ecological role in the plume ecosystem and are affected by a suite of physical, chemical, and biological environmental factors such as temperature, nutrients, and predators (Banas et al., 2009; Boicourt et al., 1987; Filippino et al., 2009, 2011; Laurent et al., 2012). These factors interplay with each other and their relative effects are not well studied in most systems (Dagg et al., 2004), which underlines the need of improved understanding of the biophysical controls on the nutrient and phytoplankton variability in these systems.

The Chesapeake Bay outflow plume (CBOP) is the coastal buoyant discharge out of Chesapeake Bay (Fig. 1), which connects the autotrophic and eutrophic bay with the heterotrophic and less eutrophic coastal ocean (Boicourt et al., 1987; Kemp et al., 2005; Smith and Kemp, 1995). Due to the relatively long estuarine residence time (Du and Shen, 2016), a considerable proportion of inorganic nutrients are assimilated into organic forms before being exported out of the bay (Boynton et al., 1995; Feng et al., 2015); for example, Kemp et al. (1997) reported a marked decrease of the dissolved inorganic nitrogen (DIN) to total organic nitrogen (TON) ratio from tributaries (5.1) to the outflow (0.04). Consequently, the surface DIN concentration in the CBOP is usually low or undetectable, and the plume and coastal waters tend to be nitrogen-limited according to a few field observations (Bates and Hansell, 1999; Filippino et al., 2009; Malone and Ducklow, 1990).

Primary productivity in the CBOP typically falls between that in estuarine and shelf waters (Malone and Ducklow, 1990), and is highly variable and influenced by the complicated nutrient transport and transformation (Filippino et al., 2009). Acker et al. (2005) ascribed the elevated chlorophyll *a* (Chl-a) out of the bay mouth to increased

* Corresponding author.
E-mail address: mxia@umes.edu (M. Xia).

https://doi.org/10.1016/j.pocean.2018.03.004
Received 2 February 2017; Received in revised form 4 March 2018; Accepted 6 March 2018
Available online 08 March 2018
0079-6611/ © 2018 Elsevier Ltd. All rights reserved.

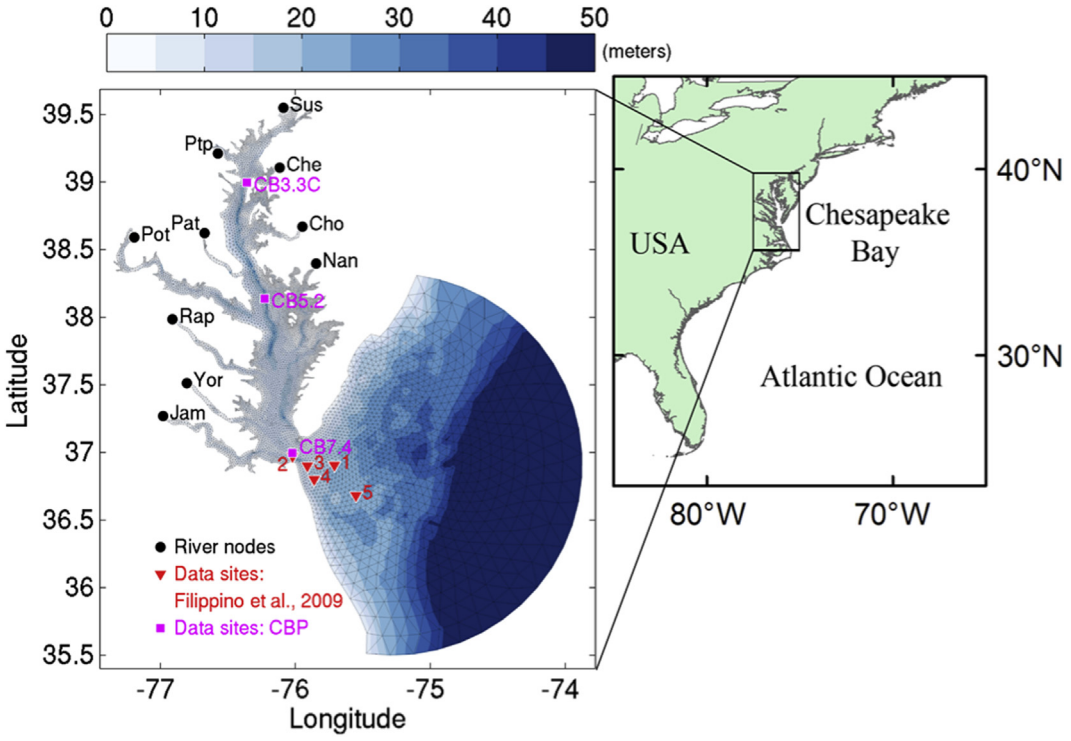

Fig. 1. Model domain, grid, bathymetry, river boundaries, and data sites of Chesapeake Bay. River nodes are marked in black dots: "Sus", Susquehanna River; "Ptp", Patapsco River; "Che", Chester River; "Cho", Choptank River; "Pat", Patuxent River; "Pot", Potomac River; "Nan", Nanticoke River; "Rap", Rappahannock River; "Yor", York River; "Jam", James River. The red triangles and pink squares indicate data sites from Filippino et al. (2009) and the Chesapeake Bay Program (CBP).

nutrient input in a wet year. However, high terrestrial input does not always accelerate algal accumulation in the CBOP, which is likely affected by physical conditions and the plume morphology (Filippino et al., 2009; Glibert et al., 1991; Malone and Ducklow, 1990). Thus far, the importance of these factors in regulating phytoplankton distribution in the plume has not been systematically studied (Filippino et al., 2009).

Our previous study revealed that winds and river discharge exerted a first-order control on the event-scale, seasonal, and interannual CBOP salinity distribution (Jiang and Xia, 2016). For instance, both high flow and southerly winds were responsible for the offshore penetration of estuarine waters (Jiang and Xia, 2016), which might be an important mechanism of seaward nutrient transport and enhanced biological activities in shelf waters. A recent numerical study supported the observed phenomenon that physical forcing was tightly coupled with the nutrient consumption and algal distribution inside Chesapeake Bay (Jiang and Xia, 2017); however, the connection between physical (salinity) and biological (phytoplankton) plumes remains to be established.

Overall, biogeochemical shipboard observations in the CBOP are scarce relative to other large plume systems, e.g., the Columbia (Banas et al., 2009) and Mississippi River plumes (Cai, 2003; Huang et al., 2013). Moreover, the limited spatial and temporal coverage of ship-based surveys (Filippino et al., 2009; Malone and Ducklow, 1990), especially compared to the extensive monitoring inside the bay, made it difficult to precisely depict the highly variable plume and complex biogeochemical processes (Dzwonkowski and Yan, 2005). Remotely sensed Chl-a data can be useful for understanding the sea-surface phytoplankton distribution, but cannot represent the underlying biogeochemical cycles (Filippino et al., 2009). Given the ecological significance of the CBOP and knowledge gaps described above, modeling assessment of these biogeochemical processes and their driving mechanisms (Xia et al., 2010, 2011; Xia and Jiang, 2015) are highly necessary. However, although multiple biogeochemical models are applied to Chesapeake Bay for eutrophication studies (Irby et al., 2016), none of them focused on the nutrient exchange and phytoplankton distribution in the plume region.

In this study, we describe the first modeling assessment of the nutrient and phytoplankton variability in the CBOP region and their biophysical regulations with an existing 3D hydrodynamic-biogeochemical model (Xia and Jiang, 2016). The model was implemented, calibrated, and validated for Chesapeake Bay and the adjacent coastal ocean using the unstructured-grid framework Finite Volume Community Ocean Model-Integrated Compartment Model (FVCOM-ICM). Herein, in order to further ensure the confidence in utilizing the model in subsequent analyses, the modeled nutrients and Chl-a near the bay mouth were verified with field data, and the simulated surface Chl-a distribution in the CBOP was compared with satellite imagery. In light of the aforementioned knowledge gaps, our study aims to (1) quantify the nutrient flux out of the bay and nutrient limitation in plume waters, (2) describe the phytoplankton spatiotemporal variability in the plume and (3) investigate the impacts of multiple environmental factors (freshwater discharge, nutrient loading, and winds) on the phytoplankton distribution in the plume.

2. Methods

2.1. The model domain and study area

Our model domain covers Chesapeake Bay and the adjacent coastal ocean on the east coast of United States (Fig. 1). Chesapeake Bay is a partially mixed drowned river valley with residence time of 90–300 days depending primarily on river flux (Du and Shen, 2016; Kemp et al., 2005; Shen and Wang, 2007). The 2000–3000 m^3/s combined freshwater discharge of the Susquehanna, Potomac, James, and other rivers (Fig. 1) feeds the large estuary (323 km long, up to 48 km wide, and 6.5 m deep on average), where the salinity ranges nearly 0–30 from the northern to southern end. The two-layer estuarine circulation within the estuary is subject to variations in freshwater discharge, winds, tides, and other forces (Fisher et al., 1988; Wang, 1979).

Table 1
Lists of streamflow stations (U.S. Geological Survey) involved in this study.

Rivers	Stations	Drainage area (mi^2)	Longitude (°N)	Latitude (°W)
Susquehanna River	01,578,310	27,100	76.1745	39.6578
Chester River	01,493,500	12.7	76.0146	39.2800
Choptank River	01,491,000	113	75.7858	38.9972
Nanticoke River	01,487,000	75.4	75.5619	38.7283
Patapsco River	01,589,035	312	76.7231	39.2273
Patuxent River	01,594,440	348	76.6937	38.9559
Potomac River	01,646,500	11,560	77.1275	38.9498
Rappahannock River	01,668,000	1595	77.5294	38.3083
	01,674,500	603	77.8139	38.5306
York River	01,673,000	1078	77.3325	37.7675
	02,042,500	251	77.0611	37.4361
James River	02,037,500	6753	77.5472	37.5631
	02,041,650	1342	77.4756	37.2250
	02,040,000	725	77.8592	37.4214

The model grid (13,299 nodes, 24,343 elements, and 11 uniform sigma levels) has a high resolution around the main channel and the bay mouth, and a relatively low resolution at the coastal open boundary, and the horizontal grid size ranges from 270 m to 20.9 km (Fig. 1).

2.2. Model description

FVCOM was utilized to simulate water elevation, temperature, salinity, circulation, and other hydrodynamic information, which offline drove the biogeochemical kinetics. The realistic external forcing included river discharge, atmospheric forcing, tides, and open boundary conditions. River discharge data were obtained from the U. S. Geological Survey (see Table 1 for the stations applied in this study). Discharge from tributaries was adjusted based on the drainage area using the methods and data of Seitz (1971) and Xu et al. (2012). The wind data were interpolated from the National Center for Environmental Prediction/North America Regional Reanalysis (NCEP/NARR) products, accessible online (http://www.esrl.noaa.gov/psd/data/gridded/data.narr.html). Other hydrodynamic data sources, calibration and validation processes, justification of model settings, and simulation of the physical plume are documented by Jiang and Xia (2016).

Processes including nutrient cycles, sediment diagenesis, and plankton growth were modeled in the biogeochemical component ICM (Kim and Khangaonkar, 2012; Jiang et al., 2015) with a time step of 30 min, which simulated 26 state variables in carbon, nitrogen, phosphorus, silicon, and dissolved oxygen (DO) cycles (Fig. 2), including total suspended solids (TSS), cyanobacteria (CYN), diatoms (DIA), dinoflagellates (DINO), microzooplankton (SZ, 20–200 μm), mesozooplankton (LZ, 0.2–20 mm), ammonia (NH4), nitrite and nitrate (NO23), phosphate (PO4), particulate inorganic phosphorus (PIP), labile/refractory dissolved/particulate organic carbon (LDOC, RDOC, LPOC, RPOC), labile/refractory dissolved/particulate organic nitrogen (LDON, RDON, LPON, RPON), labile/refractory dissolved/particulate organic phosphorus (LDOP, RDOP, LPOP, RPOP), particulate/dissolved silica (PSi/DSi), chemical oxygen demand (COD), and dissolved oxygen (DO).

Model inputs and parameters were described in a previous paper (Xia and Jiang, 2016). Here we highlighted the phytoplankton simulation (Eq. (1), Cerco and Noel, 2004) including three major phytoplankton groups in Chesapeake Bay, i.e., diatoms, dinoflagellates, and cyanobacteria (Adolf et al., 2006).

$$\frac{\partial B}{\partial t} = (G-R)B - W\frac{\partial B}{\partial z} - F_z BZ - FB \quad (1)$$

In Eq. (1), B is the biomass of a phytoplankton taxon (mg C/L, mg/L is used for all biomass units hereafter), t is the temporal coordinate (day), G and R are the growth and respiration rate respectively (day^{-1}), W is the settling velocity (m/day), z is the vertical coordinate converted from σ levels (m), F_z (L mg^{-1} day^{-1}) and F (day^{-1}) are the predation rates of zooplankton and other herbivores respectively, and Z is the zooplankton biomass (mg/L). The net primary production (*NPP*) is a function of temperature, nutrient, and light (Eq. (2), Cerco and Noel, 2004).

$$NPP = \iint \left(\frac{P_m}{CChl} \frac{I}{\sqrt{I^2 + I_k^2}} \frac{N(i)}{K_h(i) + N(i)} e^{-K_T(T-T_{opt})^2}(1-P_{res}) - Me^{-K_T'(T-T_{ref})} \right) B \, dz \, dt \quad (2)$$

In Eq. (2), P_m is the maximum photosynthetic rate (day^{-1}), *CChl* is the carbon to chlorophyll ratio, I and I_k are the instantaneous and reference radiation (mol photons m^{-2} day^{-1}), $N(i = 1, 2, or\ 3)$ is the concentration of each nutrient (nitrogen, phosphorus, and diatom-only silicon, mg/L), $K_h(i)$ is the corresponding half-saturation concentration in the Michaelis-Menten nutrient limitation function (mg/L), K_T ($°C^{-2}$) and K_T' ($°C^{-1}$) are the temperature coefficients on photosynthesis and basal respiration respectively, T_{opt} and T_{ref} are their corresponding optimal and reference temperature (°C), P_{res} is the percentage of active respiration in gross primary production, and M is the basal respiration/metabolism rate (day^{-1}). P_m, *CChl*, I_k, $K_h(i)$, K_T, T_{opt}, P_{res}, M, K_T', and T_{ref} are specified parameters varying with phytoplankton groups, while I, $N(i)$, and T are input data changing with time and space.

2.3. Observational data

Two sets of field data collected at stations in Fig. 1 were used to further validate the biogeochemical model around the bay mouth and in the CBOP region. The first dataset (http://www.chesapeakebay.net/what/data) maintained by the EPA Chesapeake Bay Program (CBP)

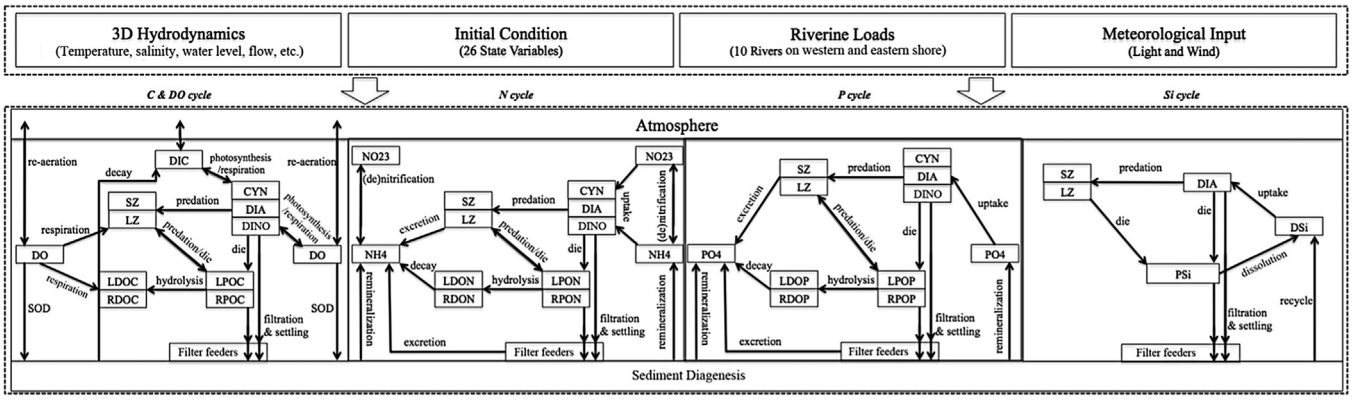

Fig. 2. Schematic flow diagram of ICM set up for Chesapeake Bay and its adjacent coastal ocean.

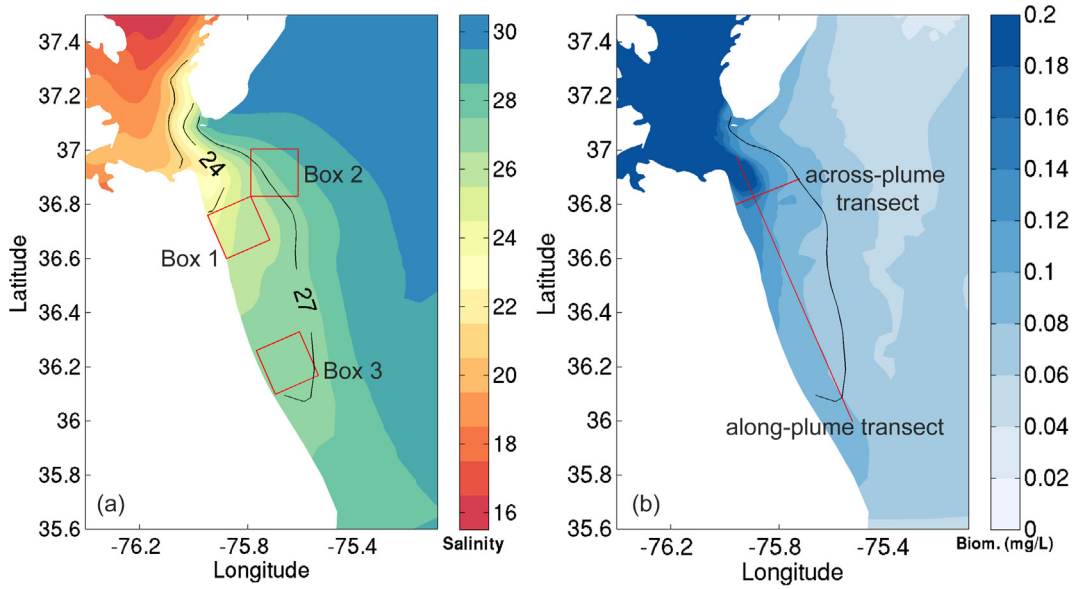

Fig. 3. Modeled surface (a) salinity and (b) phytoplankton biomass in the Chesapeake Bay outflow plume in May 2010. The phytoplankton biomass is in mg C/L, and mg/L is used for short in other figures in this study.

includes monthly monitoring nutrient and Chl-a data covering the modeling period (2003–2012) and is the primary data source to calibrate and validate our model (Xia and Jiang, 2016). Given that the CBP data are mainly inside the estuary, DIN and Chl-a data on the shelf were requested from Old Dominion University (Filippino et al., 2009), which were collected during 2005–2007 averaging five cruises each year. Additionally, the modeled surface Chl-a distribution was compared with the real-time satellite imagery (sensor: AQUA/MODIS) of the same day. Remotely sensed Chl-a images were obtained from a published study (Dzwonkowski and Yan, 2005) and NOAA Coast Watch (https://coastwatch.noaa.gov/).

2.4. Definition of the plume structure

As defined by Jiang and Xia (2016), the isohaline 27 worked as the conservative indicator of the CBOP, and the plume was the area within the isohaline 27 out of the bay mouth. For instance, Fig. 3 shows the surface salinity and phytoplankton distribution in the CBOP in May 2010 with the isohaline 27 marked. Boxes 1–3 were selected to depict the nutrient and phytoplankton variability in the inshore, offshore, and far-field parts of the CBOP (Fig. 3a), and two transects were used to reveal the biogeochemical variables along and across the plume (Fig. 3b).

2.5. Design of numerical experiments

A series of numerical experiments were conducted to examine the sensitivity of nutrients and phytoplankton in the CBOP to multiple environmental factors (Table 2). Given that the CBOP is a surface-trapped plume (Jiang and Xia, 2016), only surface nutrient and phytoplankton variability were examined in the calibration run and numerical experiments. The year 2010, with normal streamflow and winds (Jiang and Xia, 2016), worked as the baseline scenario. Generally, variations of streamflow or nutrients at the riverine end would be manifested at the bay mouth in around one month (Jiang and Xia, 2016; Sletten et al., 1999; Valle-Levinson et al., 1998a). Thus, the duration of experiments was set as one month, and the monthly average output was analyzed in each numerical scenario. In order to make the response of phytoplankton biomass to various environmental factors more detectable, all numerical experiments were based on the calibration run in May, the month with nearly the highest phytoplankton biomass of the year (Section 5).

Table 2
A list of numerical experiments in this study.

Environmental factors	Treatments
DIN loading	Scaled by 50%, 80%, 90%, 110%, 120%, and 150%
DIP loading	Scaled 50%, 80%, 90%, 110%, 120%, and 150%
Streamflow	Scaled by 50%, 80%, 90%, 110%, 120%, and 150% with nutrient loading unvaried
Southerly winds	Increasing/decreasing the magnitude on the shelf by 5 m/s, 3 m/s, and 1 m/s

To compare the roles of nitrogen and phosphorus loading, the DIN and DIP input from point, non-point, and atmospheric sources were adjusted by ± 10%, ± 20%, or ± 50%, respectively (Table 2), while the nutrient input from the open boundary stayed fixed. In our model, atmospheric loading was scaled directly as fluxes (g/day), while nutrient concentrations from the point and non-point sources were adjusted without changing the freshwater flux.

It is previously found that the CBOP structure was primarily controlled by river discharge and southerly winds (Jiang and Xia, 2016), which, therefore, were adjusted individually to test their impacts on nutrient and phytoplankton distribution (Table 2). Discharge and winds remained temporally varying when adjusted. For instance, for streamflow experiments, the discharge input of each time step (24 h) was multiplied by a scaling factor of 50%-150%, and the scaling gradient was the same as that in the nutrient experiments (Table 2). When the streamflow was scaled, nutrient loading was consistent with that in the baseline run to manifest the physical impacts only. For example, in the case of reducing river discharge by 50% (r0.50), the corresponding nutrient concentrations were doubled to ensure the overall loading unchanged.

Wind variations over the estuary could potentially affect both barotropic and baroclinic processes in the bay as well as the flow exiting the bay mouth under various mechanisms, some of which are not fully understood (Chen and Sanford, 2009; Cho et al., 2012; Chuang and Boicourt, 1989; Du and Shen, 2016; Guo and Valle-Levinson, 2008; Salas-Monreal and Valle-Levinson, 2008; Valle-Levinson et al., 1998b, 2007; Wang, 1979). In scenarios pertaining to wind forcing, if changes in winds were superimposed over both the estuary and the shelf, it would be difficult to decompose the local wind impacts on the plume

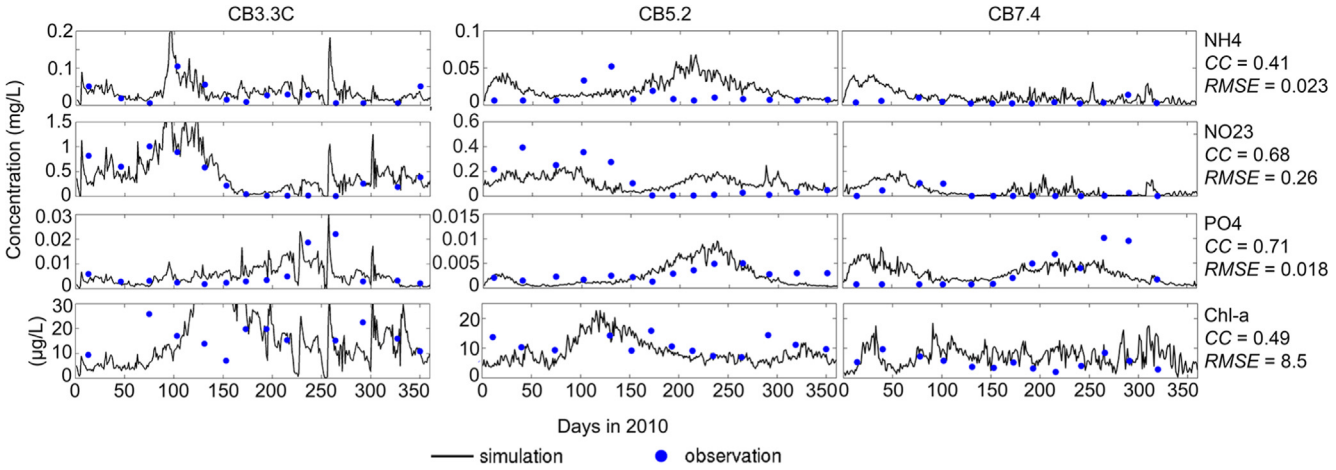

Fig. 4. Time series of observed (dots) and simulated (black solid line) nutrients and Chl-a at three sampling sites in Chesapeake Bay (Fig. 1) in 2010: NH4 (ammonia), NO23 (nitrite and nitrate), PO4 (phosphate). Data source: CBP. *CC* and *RMSE* denote the correlation coefficient ($p < 0.01$) and root mean squared error, respectively.

region from those caused by the above inner-bay processes. Hence, winds over the shelf were varied, while winds over the estuary stayed unchanged in this study (Table 2). Hereafter, winds mentioned in model validation using satellite imagery (Section 3.2), statistical analyses (Section 5), and numerical experiments (Section 6) refer to localized winds, i.e., winds over the shelf.

3. Comparison between model simulation and observational data

3.1. Comparison with field data

The CBP data and model simulation revealed that nutrient concentrations and Chl-a decreased with the distance from the Susquehanna River, the largest freshwater source of Chesapeake Bay (Figs. 1 and 4). After extensive assimilation in the estuary, a limited portion of inorganic nutrients could reach the bay mouth (CB7.4, Fig. 4). Phosphate concentration at CB7.4 maximized in late summer and fall, while the spring phytoplankton biomass (Chl-a) was slightly higher than that in other seasons (Fig. 4). However, the seasonal patterns of nutrients and Chl-a at CB7.4 were not as strong as those within the estuary (CB3.3C and CB5.2) (Fig. 4).

To corroborate the model performance of main nutrient and phytoplankton variables in the plume region, the simulated Chl-a and DIN were compared with observations near the bay mouth and on the adjacent shelf, including data from one CBP station (CB7.4) and all five stations from Filippino et al. (2009). Influenced by both biotic and abiotic factors, Chl-a (phytoplankton biomass) is usually the most challenging variable to accurately simulate in complex biogeochemical models (Robson, 2014). Linker et al. (2002) suggested that the "goodness" or "skill" of Chl-a simulation in management-oriented system models should meet certain criteria including a correlation coefficient (*CC*) over 0.45 and a standard deviation (the value close to root mean square error, *RMSE*) below 300%, and the Chl-a model performance in the plume region ($CC = 0.58$, $RMSE = 3.4$ and standard deviation = 72%, Fig. 5a) was beyond these criteria. The biogeochemical model (Xia and Jiang, 2016) performed among the best in the estuarine

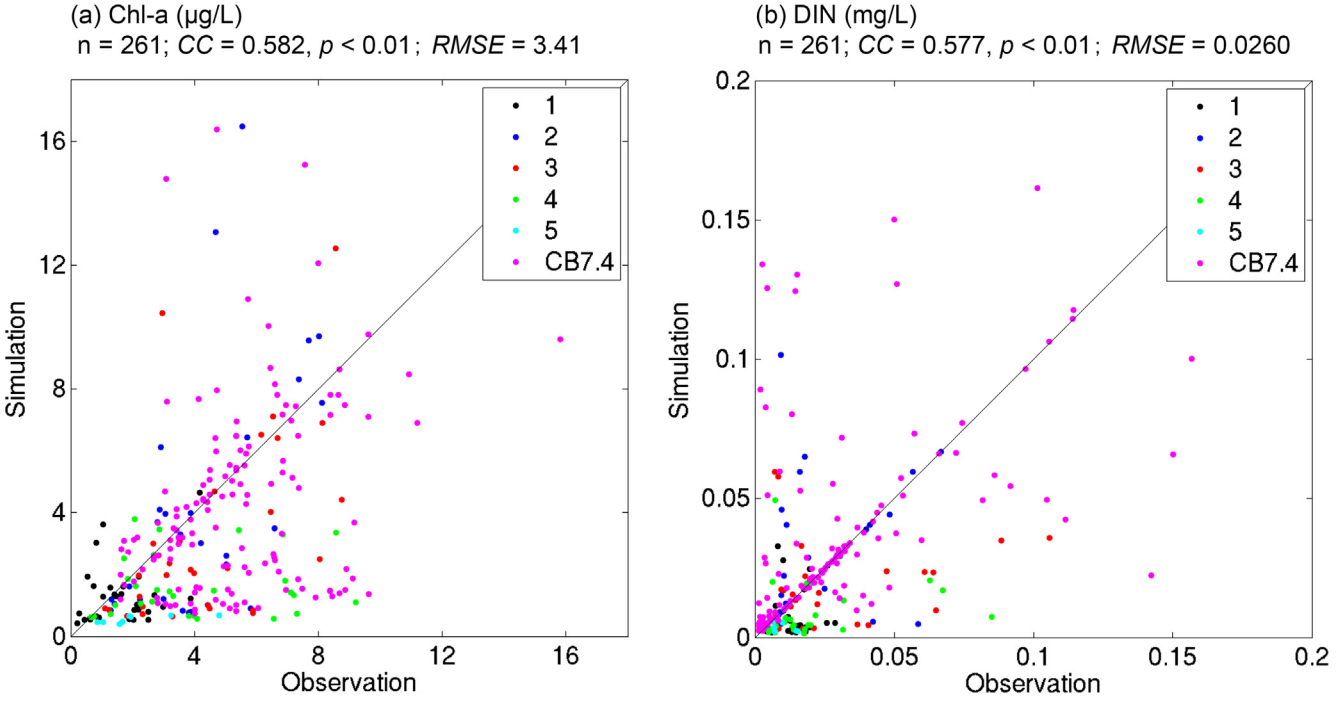

Fig. 5. Comparison between modeled and observed Chl-a and dissolved inorganic nitrogen (DIN) at stations near the bay mouth and on the shelf. Different colors of dots indicate data collected at different sites including CB7.4 and five stations from Filippino et al. (2009) (Fig. 1). *CC* and *p* denote the correlation coefficient and its *p*-value, and *RMSE* is the root mean squared error.

Chl-a simulation, according to a comparative study of multiple current biogeochemical models implemented for Chesapeake Bay (Irby et al., 2016), and the Chl-a model skill in the plume region was superior to that within the bay (CC = 0.48 and $RMSE$ = 6.2). Even though the model tended to underestimate Chl-a at relatively high observed levels (4–8 μg/L) and overestimate DIN at low observed concentrations (< 0.02 mg/L), Chl-a and DIN displayed similarly reasonable model skills in terms of CCs and $RMSE$s (Fig. 5).

3.2. Comparison between model simulation and satellite imagery

Given the scarcity of field data, satellite Chl-a imagery was used for supplemental model validation of the spatial phytoplankton distribution. The simulated surface Chl-a in the CBOP followed the general patterns in corresponding satellite images under various conditions (Fig. 6). During 12–14 April 2003, the remote sensing Chl-a images were found to capture the initial, bulge-developing, and jet-developing stages of the CBOP under downwelling-favorable winds (Dzwonkowski and Yan, 2005). In this 3-day period, both simulated and observed Chl-a evolved with the plume structure, narrowing and penetrating alongshore under persisting northerly winds (Fig. 6a–c). Similarly, the plume water with higher Chl-a compared to the shelf water was confined to the coast after a 3-day northwesterly event in February 2010, as revealed by both model simulation and satellite products (Fig. 6d). In contrast, under upwelling-favorable winds, the offshore region became abundant in phytoplankton biomass, and the mixing interface with the shelf water was extended seawards (Fig. 6e and f). These Chl-a snapshots suggested the phytoplankton redistribution in the CBOP in response to changing atmospheric conditions, which, in combination with the comparison with field data, added to the fidelity of the subsequent modeling assessment in this study.

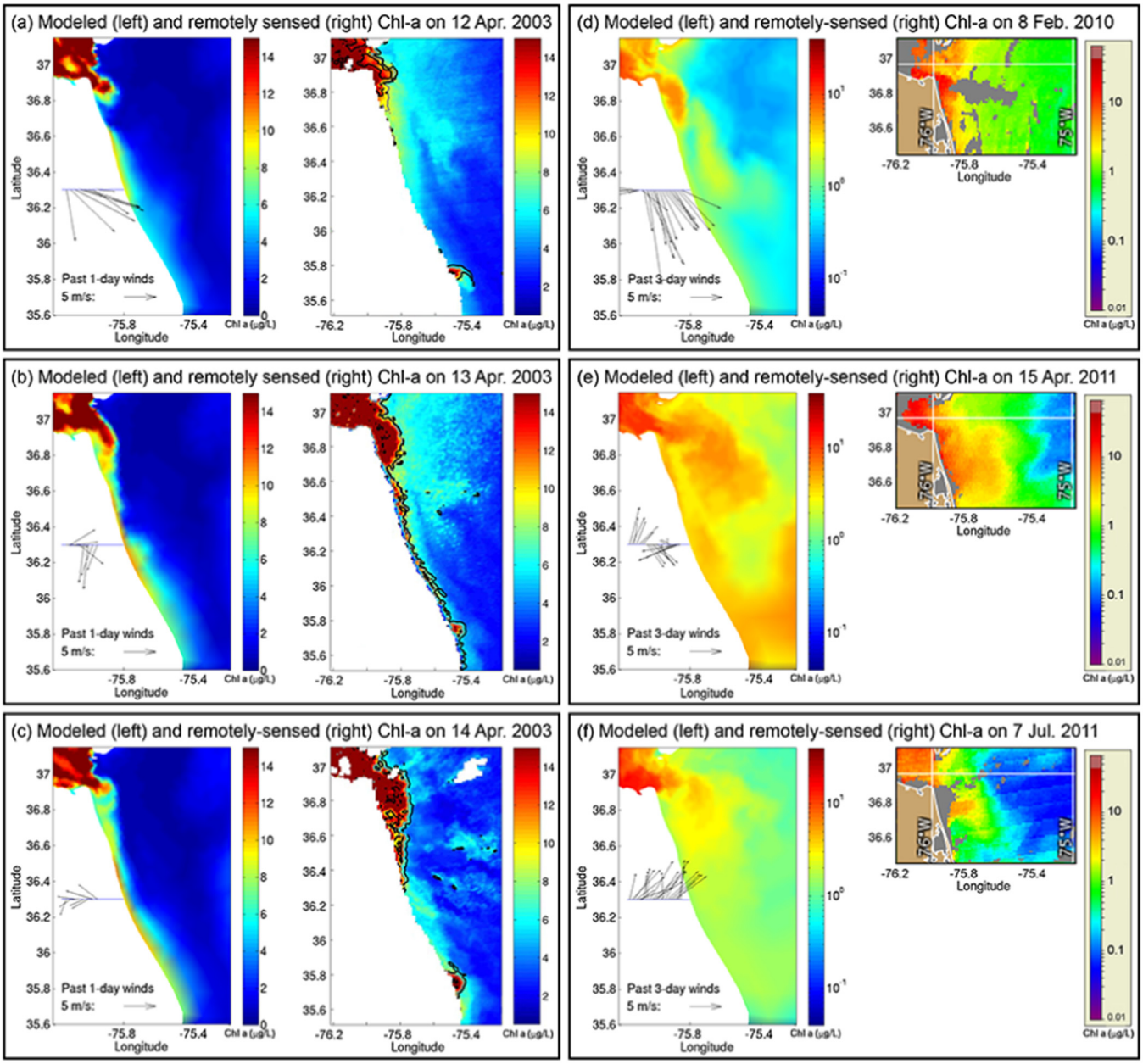
(a) Modeled (left) and remotely sensed (right) Chl-a on 12 Apr. 2003
(b) Modeled (left) and remotely sensed (right) Chl-a on 13 Apr. 2003
(c) Modeled (left) and remotely-sensed (right) Chl-a on 14 Apr. 2003
(d) Modeled (left) and remotely-sensed (right) Chl-a on 8 Feb. 2010
(e) Modeled (left) and remotely-sensed (right) Chl-a on 15 Apr. 2011
(f) Modeled (left) and remotely-sensed (right) Chl-a on 7 Jul. 2011
Past 1-day winds
Past 3-day winds
5 m/s:
Latitude
Longitude
Chl a (μg/L)
76°W
75°W

Fig. 6. The simulated surface Chl-a distribution (μg/L) in the Chesapeake Bay outflow plume region compared with satellite imagery of the same day on (a) 12 April 2003, (b) 13 April 2003, (c) 14 April 2003, (d) 8 February 2010, (e) 15 April 2011, and (f) 7 July 2011. Sources of satellite imagery: (a–c) Dzwonkowski and Yan (2005), (d–f) Coast Watch, NOAA. Winds on the shelf during in the previous day (a–c) or past three (d–f) days are shown in each panel and the interval between wind vectors is three hours.

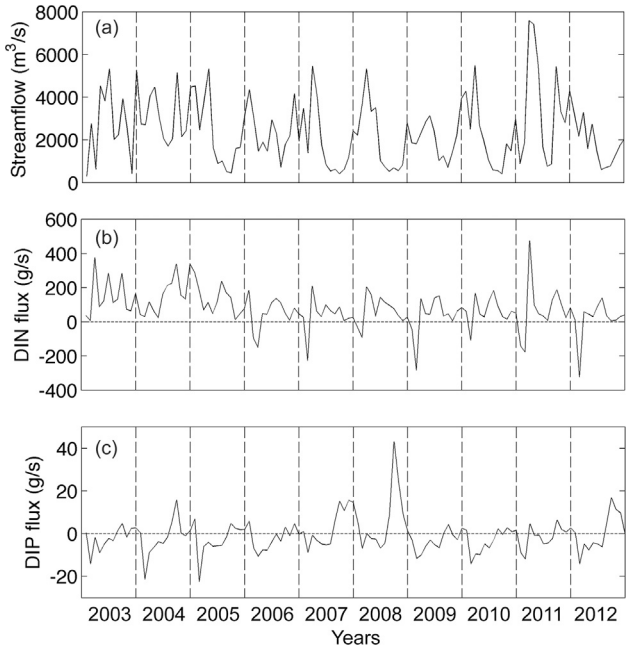

Fig. 7. Time series of (a) streamflow into Chesapeake Bay, and the simulated (b) dissolved inorganic nitrogen (DIN) and (c) phosphorus (DIP) fluxes out of the bay mouth during 2003–2012. The streamflow data were integrated from our model input using flow information from U. S. Geological Survey (See Section 2.1 and Table 1 for details), and the DIN and DIP fluxes were calculated from our model output.

4. Nutrient variability in the plume

4.1. Nutrient flux at the bay mouth

Over the 10-year simulation period, the peak streamflow occurred in spring, while high evapotranspiration contributed to the low streamflow in late summer and fall (Fig. 7a), as illustrated by Najjar (1999). At the bay mouth, the net DIN flux was typically seaward with an average of 75.6 ± 48.6 g N/s (Fig. 7b), which was among the range in literature (e.g., 0–507 g N/s, Feng et al., 2015; 101 g N/s, Kemp et al., 1997). The DIN flux accounted for a negligible fraction of the total nitrogen export since it was largely assimilated into organic forms in the bay (Feng et al., 2015; Kemp et al., 1997). Furthermore, the DIN flux exiting the bay (Fig. 7b) was significantly correlated with streamflow (correlation coefficient, $CC = 0.42$, $p < 0.05$). Two potential processes could contribute to the correlation: (1) DIN leached from the watershed as a result of higher streamflow increased the non-point-source loading, as shown by empirical data (Boynton and Kemp, 2000) and numerical models (Howarth et al., 2006), and (2) an increase in river discharge reduced the estuarine residence time (Du and Shen, 2016) and the proportion of DIN assimilated inside the estuary, and favored its export. Comparison of these two processes is discussed in Section 6.

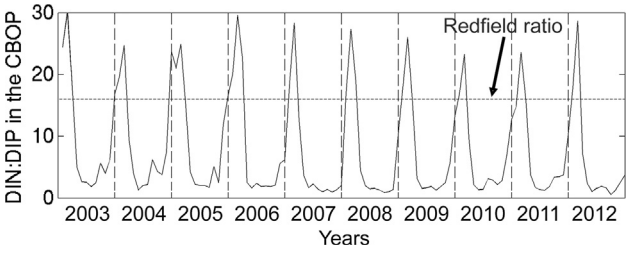

Fig. 8. The dissolved inorganic nitrogen to phosphorus (DIN:DIP) ratio in the Chesapeake Bay outflow plume during 2003–2012. The horizontal dash line denotes the Redfield ratio 16:1. See the definition of the plume in Section 2.3.

In contrast, an average of 0.8 ± 3.0 g P/s DIP flux was delivered into the bay in the study period (Fig. 7c). The net phosphorus import from the coastal ocean was observed previously (Boynton et al., 1995). The DIP export occurred mainly in late summer and fall because of the high regenerative phosphate in Chesapeake Bay (Fig. 4), supported by empirical data (Taft and Taylor, 1976). Time series of the DIP import was significantly correlated with the volume flux into the estuary ($CC = 0.59$, $p < 0.05$) rather than streamflow ($CC = -0.09$, $p > 0.10$). The imbalance between DIN and DIP transport at the bay mouth motivated us to examine the nutrient limitation in the plume.

4.2. Nitrogen limitation and variability in the plume

Within the CBOP defined by salinity (Fig. 3), the atomic ratio of DIN: DIP was well below the Redfield ratio except in early spring (Fig. 8), when the phytoplankton uptake was slow and the DIN export was high (Fig. 7). The DIN concentration in the plume was at least one order of magnitude lower than that in the bay, especially in summer and fall (Figs. 4 and 9). The strong nitrogen limitation and extremely low DIN concentration in the CBOP were reported in previous surveys (Filippino et al., 2009; Glibert et al., 1991; Malone and Ducklow, 1990), while phosphorus limitation usually prevailed in some large freshwater-dominated plumes, e.g., the Mississippi (Laurent et al., 2012) and Pearl River plumes (Yin et al., 2004).

Strong DIN spatiotemporal patterns were detected in the 10-year DIN-salinity mixing diagram along the plume (Fig. 9). The DIN concentration maximized in all seasons at the plume core (the position with the lowest salinity), which was located at the main conduit of the outflow, a deep channel near Cape Henry (Jiang and Xia, 2016). In addition to the buoyant outflow, another mixing end member was the ambient water with low DIN abundance (Fig. 9). In spring, the along-plume ranges of DIN (0.03–0.11 mg/L) and salinity (22–28) were greatest, and the DIN uptake occurred all along the transect (Fig. 9). In summer, the DIN was rapidly consumed within ~8 km (the distance between two adjacent dots was 500 m) and salinity values of 21–23 in the near field (Fig. 9). Low discharge rendered a small CBOP in fall as indicated by its narrow salinity range, and the plume DIN concentration was least abundant during fall and winter because of low estuarine export (Figs. 7 and 9). The interannual variations of salinity and DIN were greatest in summer and fall, respectively (Fig. 9).

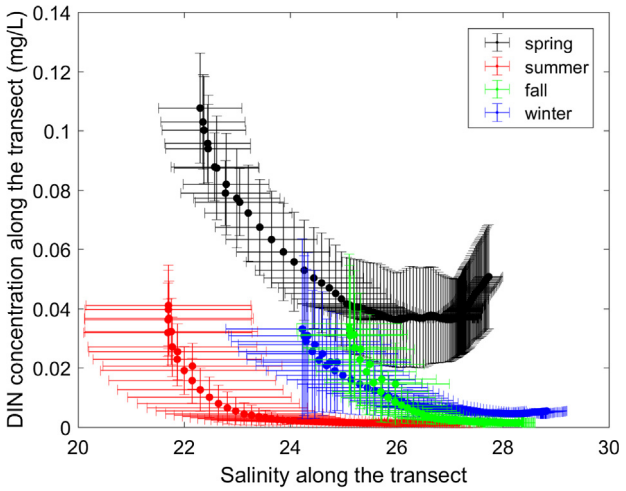

Fig. 9. Seasonal average mixing diagram of the surface dissolved inorganic nitrogen (DIN) on the along-plume transect (see Fig. 3b for the transect location) during 2003–2012. The dots represent the 10-year average values of salinity and DIN, and the error bars indicate the standard deviation. Spring, March to May; summer, June to August; fall, September to November; winter, December to February.

5. Phytoplankton variability in the plume

During the 10-year simulation period, phytoplankton biomass in different plume regions exhibited similar seasonal variations: a spring bloom during April and May and a less intense fall bloom (Fig. 10). Spatially, near field phytoplankton biomass (Box 1) was 23.1% (0.022 mg/L) higher than that in the far field (Box 3), especially in summer and fall (Fig. 10), which was in line with the DIN gradient along the plume (Fig. 9). Moreover, the near- and far-field biomass was highly correlated ($CC = 0.92$, $p < 0.05$), implying the similar regulation mechanism. The offshore (Box 2) biomass was slightly (6.2%) lower than inshore (Box 1) in the near field (Fig. 10). The offshore spring biomass was greater than inshore in some years (e.g., 2007 and 2011), but extremely low in some other years (e.g., 2003 and 2010); as a result, *CC* of biomass in these two adjacent areas was only 0.80 (Fig. 10). Malone and Ducklow (1990) observed the highest phytoplankton biomass in spring near the bay mouth and decreasing trends both alongshore and seawards, which was consistent with our results. If counting late March as spring, Filippino et al.'s data (2009) also supported the highest plume phytoplankton biomass in spring.

Phytoplankton biomass in all three regions was significantly inversely correlated with salinity (Fig. 11), which implied that the salinity plume structure might affect the algal distribution. The 10-year monthly time series of biomass in Box 1 was significantly correlated with DIN and DIP fluxes at the bay mouth, streamflow, and westerly and southerly winds (Table 3). The offshore phytoplankton abundance was mainly related to the DIP flux, freshwater discharge, and southerly winds, while algal biomass in the far field was only significantly correlated with the DIP flux and streamflow (Table 2). Given that the plume area was hardly limited by phosphorus (Fig. 8), negative correlations between the DIP flux and phytoplankton biomass (Table 3) could result from changes in the flow field rather than the DIP supply. The bay mouth DIN flux was significantly correlated with the algal biomass in Box 1 only, whereas streamflow contributed to the phytoplankton variability in all three regions investigated (Table 3). Therefore, we inferred that streamflow might have a more extensive effect on the CBOP phytoplankton dynamics than nutrient loading. Similar correlation analyses were conducted over the seasonal ($n = 12$) and interannual ($n = 10$) scales. Due to reduced data sizes, the only two significant correlations were between freshwater discharge and the far-field (Box 3) phytoplankton biomass on the seasonal scale ($CC = 0.64$, $p < 0.05$), and between southerly winds and the offshore (Box 2) biomass on the interannual scale ($CC = 0.83$, $p < 0.05$). These statistical analyses on the modeled data implied the important roles of nutrients loading, streamflow, and southerly winds in plume phytoplankton accumulation, which were further examined using numerical experiments.

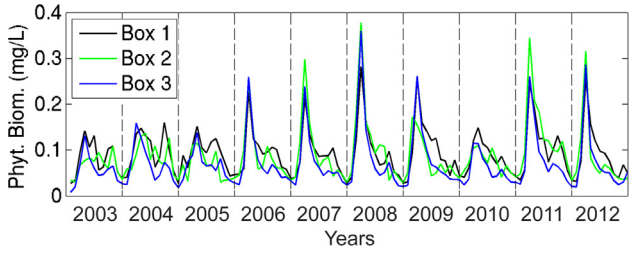

Fig. 10. The simulated phytoplankton biomass in Boxes 1–3 during 2003–2012. See Fig. 3a for box locations.

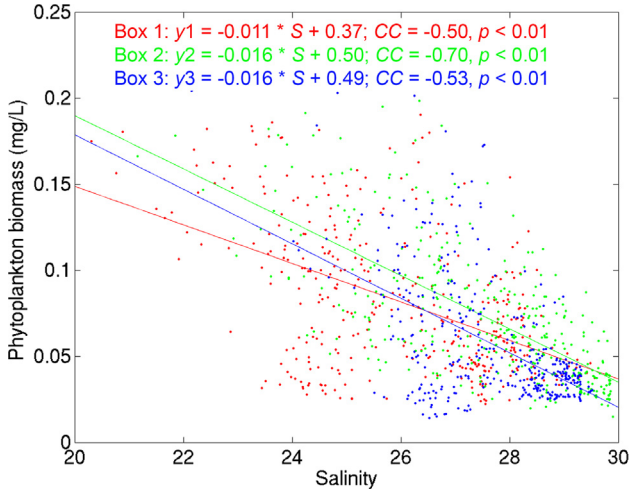

Fig. 11. Scatter plot between surface salinity and phytoplankton in Boxes 1–3 (see Fig. 3a for box locations) in 2010. The lines and equations show the best linear regression model in each pair of comparison, while *CC* and *p* are the correlation coefficients and its *p* values, respectively.

Table 3
Correlation analysis between the 10-year monthly time series of modeled phytoplankton biomass in Boxes 1–3 (see Fig. 3a for box locations) and environmental factors.

Factors		Phytoplankton biomass in Box 1	Phytoplankton biomass in Box 2	Phytoplankton biomass in Box 3
DIN flux out of the bay mouth	*CC*	0.28*	0.08	0.11
	p	< 0.05	0.20	0.11
DIP flux out of the bay mouth	*CC*	−0.21*	−0.22*	−0.26*
	p	< 0.05	< 0.05	< 0.05
Streamflow	*CC*	0.42*	0.34*	0.31*
	p	< 0.05	< 0.05	< 0.05
Westerly winds	*CC*	−0.32*	−0.01	−0.14
	p	< 0.05	0.47	0.06
Southerly winds	*CC*	0.25*	0.22*	0.12
	p	< 0.05	< 0.05	0.10

Note: n = 120; *CC*, correlation coefficient; *p*, *p* value calculated from the correlation analysis.
* Significant at the $p = 0.05$ level.

6. Sensitivity experiments

6.1. An overview of numerical experiments

Phytoplankton biomass in all examined regions increased nearly linearly with DIN loading with the greatest slope in Box 1, which supported the statistical finding that the sensitivity of phytoplankton biomass to DIN loading was highest in the near-field and inshore region of the plume (Fig. 12a-c). In contrast, adjusting DIP loading did not cause significant biomass variations (Fig. 12d-f), verifying the severe CBOP nitrogen limitation. When streamflow was scaled up with constant nutrient loading, phytoplankton biomass increased non-linearly (Fig. 12 g–i), and the increasing amplitude was greater than that with corresponding adjusted DIN loading, particularly in Boxes 2 and 3 (Fig. 12a–c). Namely, even with the same nutrient loading, the increasing river discharge could enhance algal accumulation all over the CBOP, likely through increasing nutrient export (reducing the estuarine residence time) and broadening the plume area. The response of the biomass to varying southerly winds was most prominent in offshore waters (Fig. 12j–l), which was in line with the correlation analysis. The individual impacts of these environmental factors were then examined below.

6.2. Effects of nutrient loading versus streamflow

The seaward DIN flux tended to increase with streamflow (Section 4.1), which could result from (1) increasing DIN leaching from the

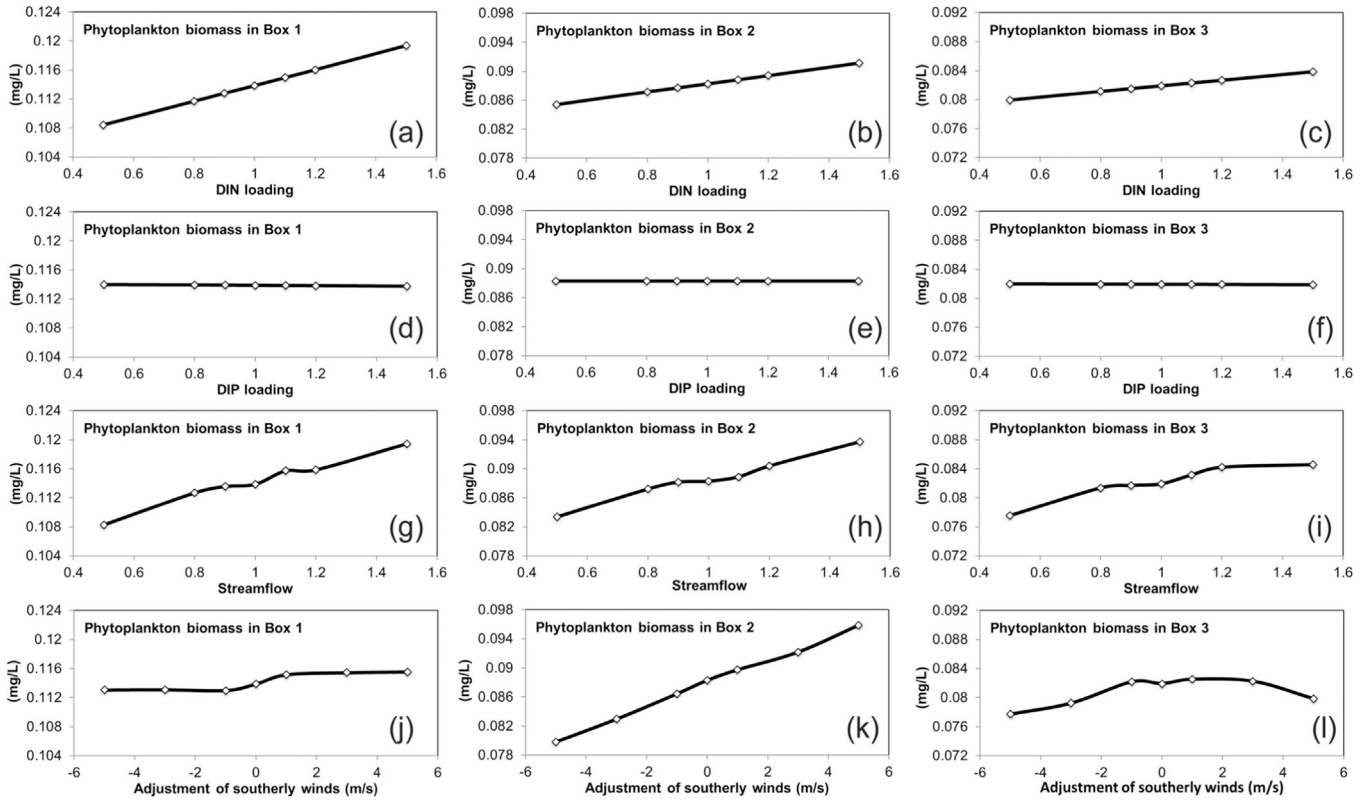

Fig. 12. Phytoplankton biomass variations in Boxes 1–3 in numerical experiments of adjusting the (a–c) dissolved inorganic nitrogen (DIN) and (d–f) phosphorus (DIP) loading, (f–i) streamflow, and (j–l) southerly winds. In panels (a–i), values on the x-axis are the relative changes, e.g., 0.8 in DIN loading denotes 80% of DIN loading were imposed in the scenario. See Table 2 for treatments of numerical experiments. Note that the y-axis ranges and tick intervals are the same among panels.

watershed and (2) reducing estuarine residence time and DIN assimilation in the bay. Our experiments aimed to decouple these effects by varying nutrient input with original streamflow (only process (1) in effect) and varying streamflow (thus, varying residence time) without changing nutrient input (only process (2) in effect), respectively. Results indicated that a decline in estuarine residence time rendered higher DIN concentrations on the shelf than those in scenarios of increasing nutrient loading only, particularly near the bay mouth (Fig. 13a, b, d, and e). Due to a relatively long distance from the bay mouth, the far-field DIN concentration showed nearly no variation with either of these factors (Fig. 13c and f). Overall, the second process, i.e., reducing estuarine residence time, seemed to exert a stronger influence on the DIN export than the first, i.e., increasing the DIN loading.

With increasing DIN loading with original streamflow, the plume structure showed no difference (Fig. 14a and b), and phytoplankton enrichment mainly occurred in the near-field and inshore region of the plume (Figs. 12 and 14e and f). In comparison, when streamflow was enlarged, the CBOP extended both alongshore and offshore (Fig. 14c and d), and its biomass increased noticeably in the far field (Fig. 14c and d) and offshore (Fig. 14g and h). Thus, streamflow could influence the CBOP phytoplankton distribution by impacting the plume signature, especially in the far-field and offshore waters. Filippino et al. (2009) speculated that the CBOP physical structure was responsible for shaping Chl-a patterns out of the bay mouth. Our study supported this conclusion and meanwhile highlighted the substantial influence of estuarine residence time on transporting inorganic nutrients onto the shelf and fueling phytoplankton accumulation, which should be a main contributor to the observed elevated Chl-a along the Chesapeake Bight in wet years (Acker et al., 2005).

6.3. Effects of southerly winds

The offshore phytoplankton biomass was most sensitive to southerly winds among other environmental factors (Fig. 12). With strengthening southerly winds, the CBOP was shortened and widened (Fig. 15a and b), and phytoplankton distribution resembled salinity variations (Fig. 15). Findings from Section 4 revealed that waters exiting the bay were primary nutrient sources to the plume and shelf. Southerly winds are effective in spreading the estuarine outflow offshore, increasing the plume size, and fertilizing the offshore waters (Jiang and Xia, 2016). Thus, biomass at the offshore end of the across-plume transect increased prominently with southerly winds (Fig. 15c–f). Over event scales, southerly winds were responsible for the offshore Chl-a enrichment (Fig. 6); significant correlations between the offshore biomass and southerly winds were detected in analyses of the monthly time series (Table 3) and over the interannual scale (Section 5). These results elucidated the critical role of southerly winds in offshore phytoplankton distribution, and special attention should be paid to local atmospheric forcing when planning and conducting future CBOP biogeochemical investigations.

Filippino et al. (2009) proposed the possible physical mechanisms in mediating algal distribution in the CBOP, for which our numerical experiments of varying streamflow and winds provided additional evidence. Specifically, the buoyant outflow was one major nutrient source on the inner shelf, and the CBOP size, structure, and behavior driven by these environmental factors dominated the nutrient transport and phytoplankton proliferation. Zooplankton and ichthyoplankton abundance within the plume area is usually tightly related to the Chl-a patterns (Boicourt et al., 1987; Grimes and Finucane, 1991; Liu and Dagg, 2003; Pagano et al., 1993). Hence, we suggest that atmospheric and hydrologic conditions should be fully considered in assessing the quality of the fish nursery habitat and feeding ground. Furthermore, streamflow and wind patterns are subject to unpredictable shifts under the ongoing climate change (Miller and Harding, 2007; Scully, 2010; Williams et al., 2010), which adds to the difficulty of understanding the future nutrient and plankton dynamics and complexity of managing the

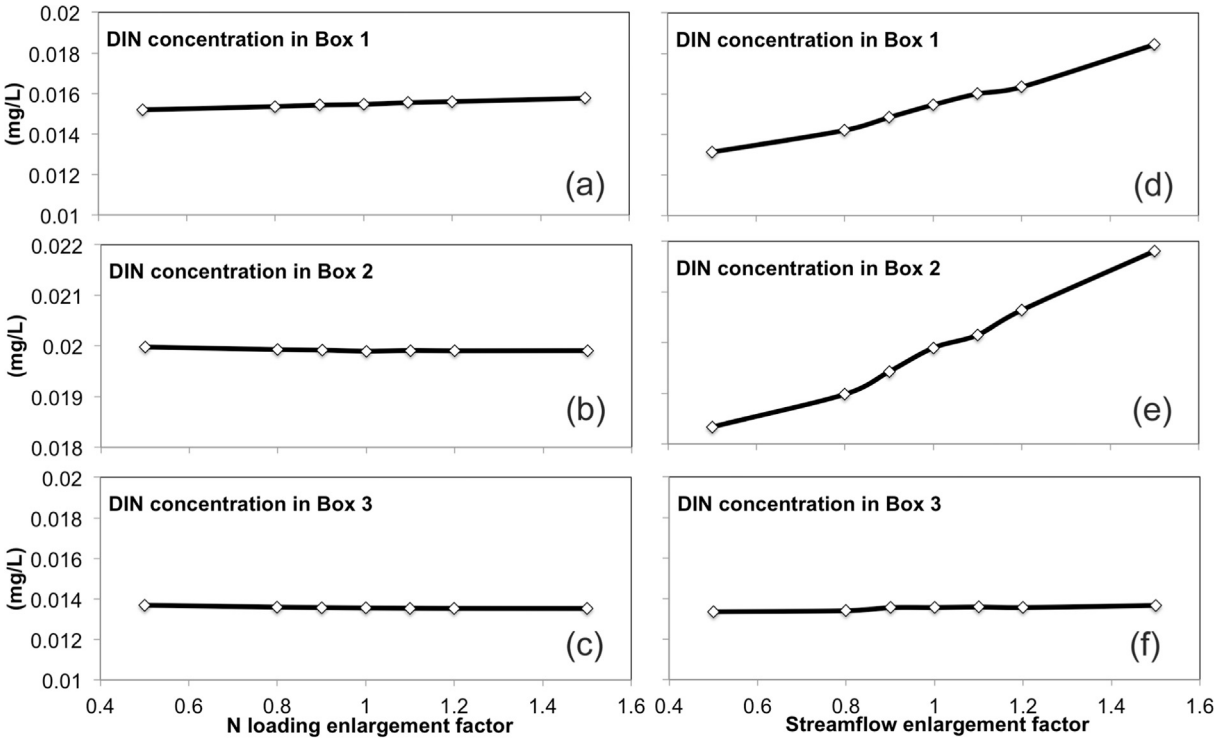

Fig. 13. Variations of surface dissolved inorganic nitrogen (DIN) concentrations in Boxes 1–3 in numerical experiments of adjusting (a–c) the DIN loading and (d-f) streamflow. See Table 2 for treatments of numerical experiments.

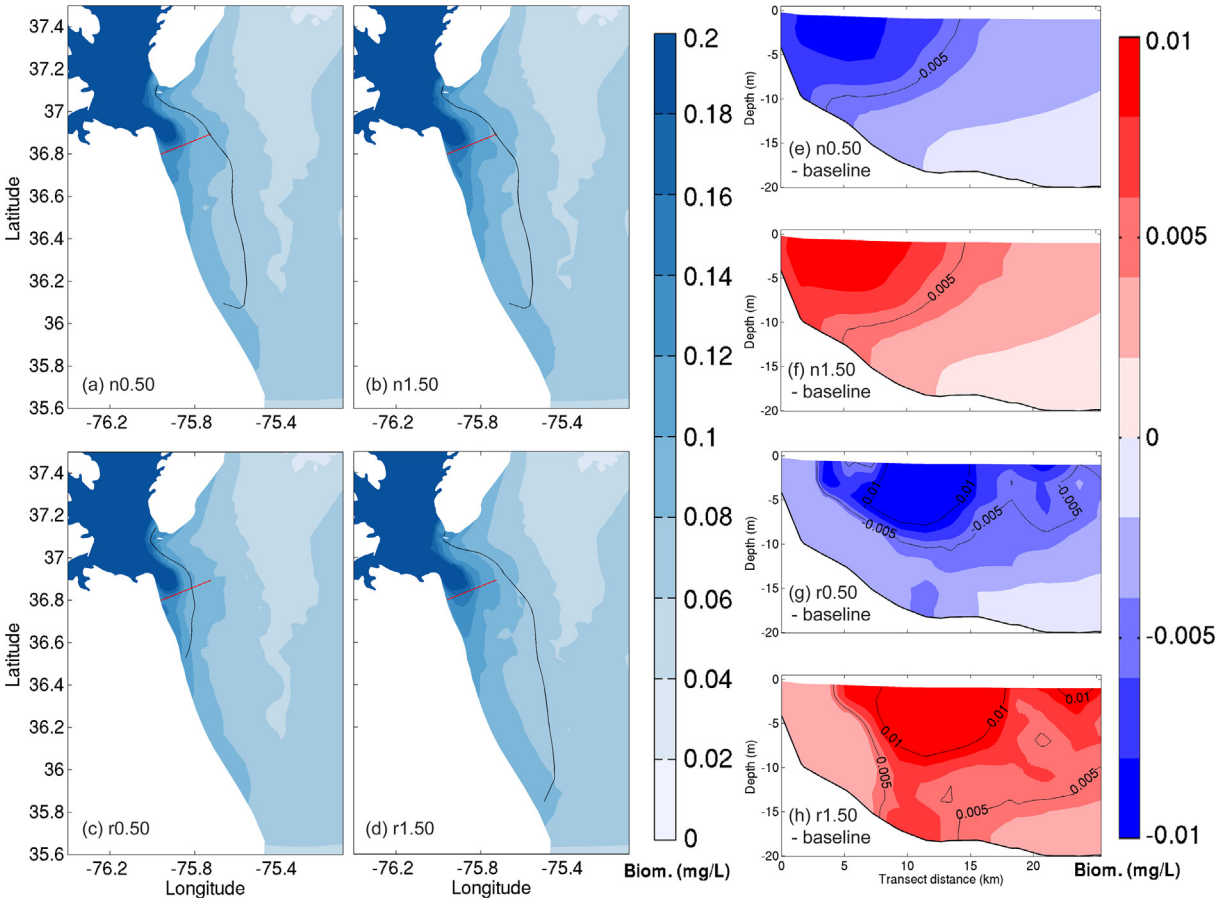

Fig. 14. (a–d) The monthly average surface phytoplankton biomass in May when decreasing and increasing the DIN loading (n0.50 and n1.50) and streamflow (r0.50 and r1.50) by 50%, and (e–h) the corresponding difference in phytoplankton biomass relative to the baseline case (Fig. 3b) on the across-plume transect. The black and red lines in panels a-d denote the 27 isohaline (indicator of the plume) and the transect across the plume, respectively. See Section 2.5 and Table 2 for description of numerical scenarios.

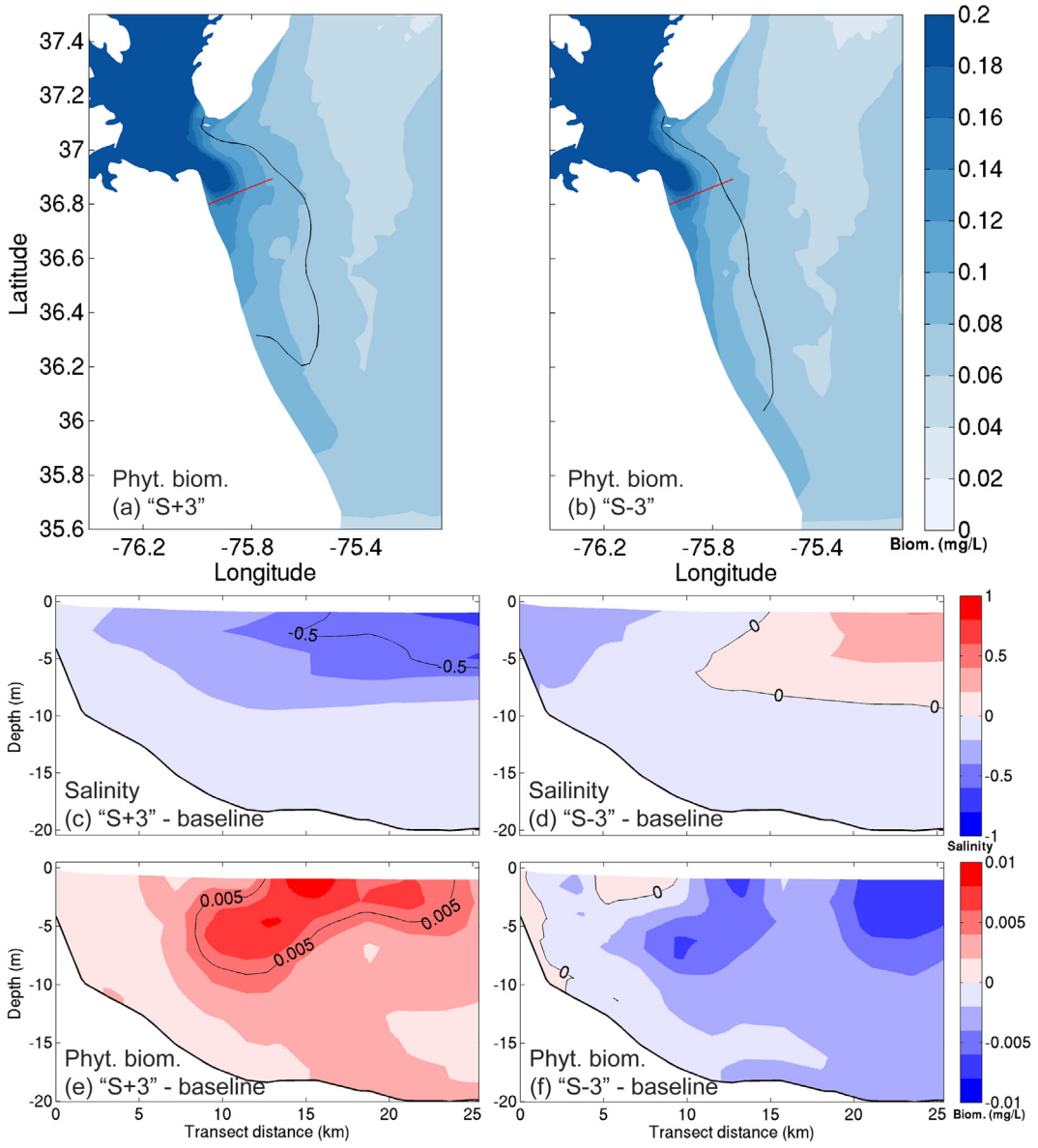

Fig. 15. The monthly average surface phytoplankton biomass in May when (a) increasing and (b) decreasing the southerly winds by 3 m/s, and differences of these two scenarios in (c, d) salinity and (e, f) phytoplankton biomass relative to the baseline case (Fig. 3) on the across-plume transect. "S + 3" and "S-3" represent the scenarios increasing and decreasing the southerly winds by 3 m/s, respectively. The black and red lines in panels (a) and (b) denote the 27 isohaline (indicator of the plume) and the transect across the plume, respectively. See Section 2.5 and Table 2 for description of numerical scenarios.

fish habitats (Grimes and Kingsford, 1996; Roman and Boicourt, 1999).

7. Summary and conclusions

We present the modeling study into nutrient and phytoplankton variability in the CBOP using the unstructured-grid hydrodynamic-biogeochemical framework FVCOM/FVCOM-ICM. The simulated nutrients and phytoplankton biomass were compared with field data and Chl-a satellite imagery during the 10-year (2003–2012) simulation to further validate the model performance in the plume region. Then, spatiotemporal patterns of nutrient and phytoplankton were analyzed and their response to multiple environmental factors was examined with statistical analyses and numerical experiments. Major conclusions are summarized as follows.

The DIN flux at the bay mouth was mostly seaward, while the net DIP flux was into the estuary. DIN export was largely affected by the estuarine residence time, and thus significantly correlated with variations of tributary discharge. As a result of intensive DIN assimilation in the estuary, the plume waters were predominately limited by nitrogen except in early spring, a period with relatively low phytoplankton uptake and high river runoff. The DIN-salinity mixing diagrams along the plume displayed strong seasonality and indicated the highest DIN consumption rate near its source, the bay mouth.

The peak phytoplankton biomass appeared during April to May in the plume. The near field was featured by higher algal abundance than the far field due to a closer distance from the nutrient source, and the inshore phytoplankton biomass was slightly greater than the offshore. Statistical analyses and numerical experiments revealed that the biomass in the far-field and offshore waters was more extensively influenced by streamflow than nutrient loading. In addition to mediating estuarine residence time and nutrient outflow, river discharge fluctuations resulted in plume structure variations, which affected corresponding algal distribution. Local southerly winds were effective in delivering high-nutrient plume waters seawards and promoting phytoplankton accumulation offshore.

Our study highlighted multiple mechanisms in regulating CBOP

phytoplankton distribution. Further (ship-based and remote sensing) biogeochemical observations in this area are encouraged to examine the above processes. In addition, the CBOP structure and its regional circulation were found very susceptible to large-scale climatic variability under climate change (Jiang and Xia, 2016), which, according to findings in this study, would very likely impact the lower food web dynamics of the estuarine plume ecosystem. The direction and amplitude of potential shifts in nutrient budget and algal activities require further investigation.

Acknowledgements

Comments from two anonymous reviewers and editors are highly appreciated. The authors thank Drs. Katherine C. Filippino and Margaret R. Mulholland for sharing the observational data. Numerical simulations were performed on the Stampede system of the Texas Advanced Computing Center (project TG-OCE120008, support to M. Xia) and the Yellowstone system of the Computational & Information Systems Laboratory, National Center for Atmospheric Research (project UMES0005, support to M. Xia and L. Jiang). This project is partially supported by the Delmarva Land Grant Institution Cooperative Seed Grant Program with funds from the USDA NIFA Evans-Allen grant. L. Jiang was partially supported by a Department Teaching Assistantship.

Appendix A. Supplementary material

Supplementary data associated with this article can be found, in the online version, at http://dx.doi.org/10.1016/j.pocean.2018.03.004.

References

Acker, J.G., Harding, L.W., Leptoukh, G., Zhu, T., Shen, S., 2005. Remotely-sensed chl *a* at the Chesapeake Bay mouth is correlated with annual freshwater flow to Chesapeake Bay. Geophys. Res. Lett. 32, L05601.

Adolf, J.E., Yeager, C.L., Miller, W.D., Mallonee, M.E., Harding, L.W., 2006. Environmental forcing of phytoplankton floral composition, biomass, and primary productivity in Chesapeake Bay USA. Estuar. Coast. Shelf Sci. 67 (1), 108–122.

Banas, N.S., Lessard, E.J., Kudela, R.M., MacCready, P., Peterson, T.D., Hickey, B.M., Frame, E., 2009. Planktonic growth and grazing in the Columbia River plume region: a biophysical model study. J. Geophys. Res. 114, C00B06.

Bates, N.R., Hansell, D.A., 1999. A high resolution study of surface layer hydrographic and biogeochemical properties between Chesapeake Bay and Bermuda. Mar. Chem. 67 (1), 1–16.

Boicourt, W.C., Chao, S.-Y., Ducklow, H.W., Glibert, P.M., Malone, T.C., Roman, M.R., Sanford, L.P., Fuhrman, J.A., Garside, C., Garvine, R.W., 1987. Physics and microbial ecology of a buoyant estuarine plume on the continental shelf. Eos. Trans. AGU 68, 666–668.

Boynton, W.R., Garber, J.H., Summers, R., Kemp, W.M., 1995. Inputs, transformations, and transport of nitrogen and phosphorus in Chesapeake Bay and selected tributaries. Estuaries 18 (1), 285–314.

Boynton, W.R., Kemp, W.M., 2000. Influence of river flow and nutrient loads on selected ecosystem processes: a synthesis of Chesapeake Bay data. In: Hobbie, J.E. (Ed.), Estuarine Science: A Synthetic Approach to Research and Practice. Island Press, Washington, D.C., pp. 269–298.

Cai, W.-J., 2003. Riverine inorganic carbon flux and rate of biological uptake in the Mississippi River plume. Geophys. Res. Lett. 30 (2), 1032.

Cerco, C.F., Noel, M.R., 2004. Process-based primary production modeling in Chesapeake Bay. Mar. Ecol. Prog. Ser. 282, 45–58.

Chen, S.N., Sanford, L.P., 2009. Axial wind effects on stratification and longitudinal salt transport in an idealized, partially mixed estuary. J. Phys. Oceanogr. 39 (8), 1905–1920.

Cho, K.H., Wang, H.V., Shen, J., Valle-Levinson, A., Teng, Y.C., 2012. A modeling study on the response of Chesapeake Bay to hurricane events of Floyd and Isabel. Ocean Model. 49, 22–46.

Chuang, W.S., Boicourt, W.C., 1989. Resonant seiche motion in the Chesapeake Bay. J. Geophys. Res. Oceans 94 (C2), 2105–2110.

Dagg, M., Benner, R., Lohrenz, S., Lawrence, D., 2004. Transformation of dissolved and particulate materials on continental shelves influenced by large rivers: plume processes. Cont. Shelf Res. 24 (7), 833–858.

Du, J., Shen, J., 2016. Water residence time in Chesapeake Bay for 1980–2012. J. Mar. Syst. 164, 101–111.

Dzwonkowski, B., Yan, X.-H., 2005. Tracking of a Chesapeake Bay estuarine outflow plume with satellite-based ocean color data. Cont. Shelf Res. 25 (16), 1942–1958.

Feng, Y., Friedrichs, M.A., Wilkin, J., Tian, H., Yang, Q., Hofmann, E.E., Wiggert, J.D., Hood, R.R., 2015. Chesapeake Bay nitrogen fluxes derived from a land-estuarine ocean biogeochemical modeling system: Model description, evaluation, and nitrogen budgets. J. Geophys. Res. Biogeosci. 120 (8), 1666–1695.

Filippino, K.C., Bernhardt, P.W., Mulholland, M.R., 2009. Chesapeake Bay plume morphology and the effects on nutrient dynamics and primary productivity in the coastal zone. Estuaries Coasts 32 (3), 410–424.

Filippino, K.C., Mulholland, M.R., Bernhardt, P.W., 2011. Nitrogen uptake and primary productivity rates in the Mid-Atlantic Bight (MAB). Estuar. Coast. Shelf Sci. 91 (1), 13–23.

Fisher, T.R., Harding, L.W., Stanley, D.W., Ward, L.G., 1988. Phytoplankton, nutrients, and turbidity in the Chesapeake, Delaware, and Hudson estuaries. Estuar. Coast. Shelf Sci. 27 (1), 61–93.

Glibert, P.M., Garside, C., Fuhrman, J.A., Roman, M.R., 1991. Dependent coupling of inorganic and organic nitrogen uptake and regeneration in the plume of the Chesapeake Bay estuary and its regulation by large heterotrophs. Limnol. Oceanogr. 36 (5), 895–909.

Grimes, C.B., Finucane, J.H., 1991. Spatial distribution and abundance of larval and juvenile fish, chlorophyll and macrozooplankton around the Mississippi River discharge plume, and the role of the plume in fish recruitment. Mar. Ecol. Prog. Ser. 75, 109–119.

Grimes, C.B., Kingsford, M.J., 1996. How do riverine plumes of different sizes influence fish larvae: do they enhance recruitment? Mar. Freshwater Res. 47 (2), 191–208.

Guo, X., Valle-Levinson, A., 2008. Wind effects on the lateral structure of density-driven circulation in Chesapeake Bay. Cont. Shelf Res. 28 (17), 2450–2471.

Herrmann, M., Najjar, R.G., Kemp, W.M., Alexander, R.B., Boyer, E.W., Cai, W.J., Griffth, P.C., Kroeger, K.D., McCallister, S.L., Smith, R.A., 2015. Net ecosystem production and organic carbon balance of US East Coast estuaries: A synthesis approach. Global Biogeochem. Cycles 29 (1), 96–111.

Howarth, R.W., Swaney, D.P., Boyer, E.W., Marino, R., Jaworski, N., Goodale, C., 2006. The influence of climate on average nitrogen export from large watersheds in the Northeastern United States. Biogeochemistry 79 (1–2), 163–186.

Huang, W.-J., Cai, W.-J., Castelao, R.M., Wang, Y., Lohrenz, S.E., 2013. Effects of a wind-driven cross-shelf large river plume on biological production and CO_2 uptake on the Gulf of Mexico during spring. Limnol. Oceanogr. 58 (5), 1727–1735.

Irby, I.D., et al., 2016. Challenges associated with modeling low-oxygen waters in Chesapeake Bay: a multiple model comparison. Biogeosciences 13, 2011–2028.

Jiang, L., Xia, M., Ludsin, S.A., Rutherford, E.S., Mason, D.M., Jarrin, J.M., Pangle, K.L., 2015. Biophysical modeling assessment of the drivers for plankton dynamics in dreissenid-colonized western Lake Erie. Ecol. Model. 308, 18–33.

Jiang, L., Xia, M., 2016. Dynamics of the Chesapeake Bay outflow plume: Realistic plume simulation and its seasonal and interannual variability. J. Geophys. Res. Oceans 121, 1424–1445.

Jiang, L., Xia, M., 2017. Wind effects on the spring phytoplankton dynamics in the middle reach of the Chesapeake Bay. Ecol. Model. 363, 68–80.

Kemp, W.M., Smith, E.M., Marvin-DiPasquale, M., Boynton, W.R., 1997. Organic carbon balance and net ecosystem metabolism in Chesapeake Bay. Mar. Ecol. Prog. Ser 150, 229–248.

Kemp, W.M., et al., 2005. Eutrophication of Chesapeake Bay: historical trends and ecological interactions. Mar. Ecol. Prog. Ser. 303, 1–29.

Kim, T., Khangaonkar, T., 2012. An offline unstructured biogeochemical model (UBM) for complex estuarine and coastal environments. Environ. Modell. Softw. 31, 47–63.

Laurent, A., Fennel, K., Hu, J., Hetland, R., 2012. Simulating the effects of phosphorus limitation in the Mississippi and Atchafalaya River plumes. Biogeosciences 9 (11), 4707–4723.

Linker, L.C., Shenk, G.W., Wang, P., Cerco, C.F., Butt, A.J., Tango, P.J., Savidge, R.W., 2002. A comparison of the Chesapeake Bay Estuary Model calibration with 1985–1994 observed data and method of application to water quality criteria. Modeling Subcommittee of the Chesapeake Bay Program, Annapolis, MD, USA.

Liu, H., Dagg, M., 2003. Interactions between nutrients, phytoplankton growth, and micro-and mesozooplankton grazing in the plume of the Mississippi River. Mar. Ecol. Prog. Ser. 258, 31–42.

Malone, T.C., Ducklow, H.W., 1990. Microbial biomass in the coastal plume of Chesapeake Bay: Phytoplankton-bacterioplankton relationships. Limnol. Oceanogr. 35 (2), 296–312.

Miller, W.D., Harding, L.W., 2007. Climate forcing of the spring bloom in Chesapeake Bay. Mar. Ecol. Prog. Ser. 331, 11–22.

Najjar, R.G., 1999. The water balance of the Susquehanna River Basin and its response to climate change. J. Hydrol. 219 (1), 7–19.

Pagano, M., Gaudy, R., Thibault, D., Lochet, F., 1993. Vertical migrations and feeding rhythms of mesozooplanktonic organisms in the Rhone River plume area (North-West Mediterranean Sea). Estuar. Coast. Shelf Sci. 37 (3), 251–269.

Robson, B.J., 2014. State of the art in modelling of phosphorus in aquatic systems: review, criticisms and commentary. Environ. Model. Softw. 61, 339–359.

Roman, M.R., Boicourt, W.C., 1999. Dispersion and recruitment of crab larvae in the Chesapeake Bay plume: Physical and biological controls. Estuaries 22, 563–574.

Salas-Monreal, D., Valle-Levinson, A., 2008. Sea-level slopes and volume fluxes produced by atmospheric forcing in estuaries: Chesapeake Bay case study. J. Coast. Res. 24 (sp2), 208–217.

Scully, M.E., 2010. The importance of climate variability to wind-driven modulation of hypoxia in Chesapeake Bay. J. Phys. Oceanogr. 40 (6), 1435–1440.

Seitz, R.C., 1971. Drainage area statistics for Chesapeake Bay fresh-water drainage basin, Chesapeake Bay Institute Special Report 19. Johns Hopkins University, Baltimore, MD.

Shen, J., Wang, H.V., 2007. Determining the age of water and long-term transport timescale of the Chesapeake Bay. Estuar. Coast. Shelf Sci. 74 (4), 585–598.

Sletten, M.A., Marmorino, G.O., Donato, T.F., McLaughlin, D.J., Twarog, E., 1999. An airborne, real aperture radar study of the Chesapeake Bay outflow plume. J. Geophys. Res. 104 (C1), 1211–1222.

Smith, E.M., Kemp, W.M., 1995. Seasonal and regional variations in plankton community production and respiration for Chesapeake Bay. Mar. Ecol. Prog. Ser. 116 (1), 217–231.
Taft, J.L., Taylor, W.R., 1976. Phosphorus dynamics in some coastal plain estuaries. In: Wiley, M. (Ed.), Estuarine Processes: Uses, Stresses, and Adaptation to the Estuary. Academic Press, New York, pp. 79–89.
Valle-Levinson, A., Li, C., Royer, T.C., Atkinson, L.P., 1998a. Flow patterns at the Chesapeake Bay entrance. Cont. Shelf Res. 18, 1157–1177.
Valle-Levinson, A., Miller, J.L., Wheless, G.H., 1998b. Enhanced stratification in the lower Chesapeake Bay following northeasterly winds. Cont. Shelf Res. 18 (13), 1631–1647.
Valle-Levinson, A., Holderied, K., Li, C., Chant, R.J., 2007. Subtidal flow structure at the turning region of a wide outflow plume. J. Geophys. Res. Oceans 112 (C4).
Wang, D.-P., 1979. Wind-driven circulation in the Chesapeake Bay, winter 1975. J. Phys. Oceanogr. 9, 564–572.
Williams, M.R., Filoso, S., Longstaff, B.J., Dennison, W.C., 2010. Long-term trends of water quality and biotic metrics in Chesapeake Bay: 1986 to 2008. Estuaries Coasts 33 (6), 1279–1299.
Xia, M., Craig, P.M., Schaeffer, B., Stoddard, A., Liu, Z., Peng, M., Zhang, H., Wallen, C.M., Bailey, N., Mandrup-Poulsen, J., 2010. Influence of physical forcing on bottom-water dissolved oxygen within Caloosahatchee River Estuary, Florida. J. Environ. Eng. 136 (10), 1032–1044.
Xia, M., Craig, P.M., Wallen, C.M., Stoddard, A., Mandrup-Poulsen, J., Peng, M., Schaeffer, B., Liu, Z., 2011. Numerical simulation of salinity and dissolved oxygen at Perdido Bay and adjacent coastal ocean. J. Coast. Res. 27 (1), 73–86.
Xia, M., Jiang, L., 2015. Influence of wind and river discharge on the hypoxia in a shallow bay. Ocean Dyn. 65 (5), 665–678.
Xia, M., Jiang, L., 2016. Application of an unstructured grid-based water quality model to Chesapeake Bay and its adjacent coastal ocean. J. Mar. Sci. Eng. 4 (3), 52.
Xu, J., Long, W., Wiggert, J.D., Lanerolle, L.W., Brown, C.W., Murtugudde, R., Hood, R.R., 2012. Climate forcing and salinity variability in Chesapeake Bay, USA. Estuar. Coasts 35 (1), 237–261.
Yin, K., Song, X., Sun, J., Wu, M.C., 2004. Potential P limitation leads to excess N in the Pearl River estuarine coastal plume. Cont. Shelf Res. 24 (16), 1895–1907.